Upconversion in a d–f [RuYb 3] Supramolecular Assembly

Richard Knighton, Lohona Soro, Waygen Thor, Jean-Marc Strub, Sarah Cianférani, Yves Mély, Marc Lenertz, Ka-Leung Wong, Carlos Platas-Iglesias, Frédéric Przybilla, et al.

Upconversion in a *d-f* [$RuYb_3$] Supramolecular Assembly

Richard C. Knighton,*,‡ Lohona K. Soro,‡ Waygen Thor, Jean-Marc Strub, Sarah Cianférani, Yves Mély, Marc Lenertz, Ka-Leung Wong, Carlos Platas-Iglesias, Frédéric Przybilla, Loïc J. Charbonnière*

We have prepared a hetero-tetrametallic assembly consisting of three ytterbium ions coordinated to a central $[Ru(bpm)_3]^{2+}$ (bpm = 2,2'-bipyrimidine) motif. Irradiation into the absorption band of the peripheral ytterbium ions at 980 nm engenders emission of the ^{3}MLCT state of the central $[Ru(bpm)_3]^{2+}$ core at 636 nm, which represents the first example of *f→d* molecular upconversion (UC). Time-resolved measurements reveal a slow rise of the UC emission, which was modeled with a mathematic treatment of the observed kinetics according to a cooperative photosensitization mechanism using a virtual Yb centered doubly excited state followed by energy transfer to the Ru centered ^{1}MLCT state.

Efficiently piling up photons in molecular or supramolecular assemblies to generate upconversion (UC)[1–3] in solution, particularly in water,[4] is still a challenge of modern chemistry. Since the pioneering work of Piguet and co-workers in 2011,[5] only few examples have still been reported,[6–10] but this burgeoning field sees each new iteration as a step forward towards better molecular UC devices. Except for the rare cases of molecular UC based on triplet-triplet annihilation (TTA) with organic dyes,[11] all examples rely on successive ascendances of the energy ladder using long-lived *d-d* or *f-f* electronic transitions, sometimes using indirect excitation by an organic near-infrared (NIR) absorbing dye.[12,13] This is typically the case for the Cr to Er energy transfer in hetero-trinuclear [Cr_2ErL_3] helicates,[5] in solution-state Yb to Tb[13,14] and Yb to Er[14–16] UC within hetero-polynuclear assemblies, or for Yb to Cr in solid mixtures.[17] Interestingly, Howard and Turshatov reported an atypical case of UC using Yb sensitizers generating TTA by energy transfer from the Yb excited state to the triplet level of a rubrene annihilator.[18] Although the system could not be considered as a single molecular entity *stricto sensu* - with no covalent or supramolecular interactions between the Yb complex and rubrene - this judicious choice allowed for the UC emission of rubrene at 559 nm upon excitation of Yb at 980 nm, through collisional energy transfer from Yb to the rubrene triplet state.

In our search for improved molecular UC devices, we hypothesized that a metal-based charge transfer transition might be of interest to increase UC efficiency. In contrast to Laporte's forbidden *d-d* and *f-f* transitions, metal to ligand or ligand to metal charge transfer transitions (respectively MLCT and LMCT) are allowed transitions and feature broad absorption (and emission) bands with large absorption cross sections reaching several thousands of $M^{-1}.cm^{-1}$. This compares favorably with Tb which has forbidden absorptions where typically $\varepsilon < 1$ $M.cm^{-1}$.[19] In addition, some of these complexes exhibit high luminescence quantum yields for metals such as Ru(II),[20] Ir(III),[21,22] or Pt(II),[23,24] and have applications in photocatalysis.[25] As the absorption arises from ^{1}CT bands, the heavy atom effect facilitates intersystem crossing to the ^{3}CT state, and the emission is significantly shifted from the absorption (*i.e.* large *pseudo*-Stokes' shift). As an example, the absorption spectrum of the archetypical photoactive transition-metal complex $[Ru(bipy)_3]^{2+}$ (bipy = 2,2'-bipyridine) has an absorption maximum at 452 nm, with a molar absorption coefficient of 14 000 $M^{-1}.cm^{-1}$ and a full width at half maximum (FWHM) of 2300 cm^{-1}, while the emission is observed as a broad band centred around 630 nm.[26] Within the frame of Förster's theory of dipole-dipole energy transfer,[27] the energy transfer rate constant, k_{ET}, is proportional to the overlap integral J between the donor emission spectrum, $I_D(\lambda)$, normalized to unity, and the acceptor absorption spectrum, defined by $\varepsilon(\lambda)$.

$$k_{ET} \propto J = \int \overline{I_D(\lambda)}\, \varepsilon(\lambda)\lambda^4 d\lambda \qquad (1)$$

$$\overline{I_D(\lambda)} = \frac{I_D(\lambda)}{\int I_D(\lambda) d\lambda} \qquad (2)$$

Hence, the larger the $\varepsilon(\lambda)$ values and the FWHM of the absorption band of the acceptor, the more efficient the energy transfer. The role of Yb as an energy relay in UC devices remains enigmatic, considering that Yb only has a single excited state at *ca.* 980 nm for the $^2F_{5/2} \leftarrow {}^2F_{7/2}$ electronic transition. In the presence of energy acceptors possessing energy levels in the NIR, as for Er for example,[28] Yb* can act as an energy donor - transferring its energy step-by-step to the acceptor, as is the case in energy transfer upconversion (ETU) processes. However, Yb can surprisingly also be an efficient sensitizer even if the acceptor doesn't possess isoenergetic levels. The case of Tb cooperative sensitization[4] is a prototypical example in which two Yb excited states cooperatively transfer their energy to a single Tb acceptor (**Scheme 1a**). Even more surprising, solid-state clusters (envisaged as polynuclear assemblies in a general sense[29]) of Yb are prone to generate cooperative luminescence according to the diagram depicted in **Scheme 1b**.[30]

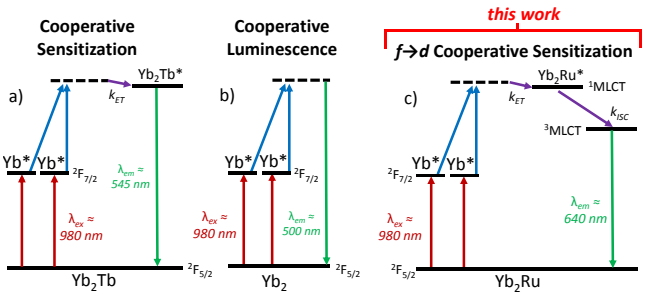

Scheme 1. Representation of the energy transfer UC process, (a) Cooperative Sensitization (CS) UC in polynuclear Yb/Tb

clusters. (b) Cooperative Luminescence (CS) by Yb. (c) Proposed *f*→*d* Cooperative Sensitization in polynuclear Yb/Ru

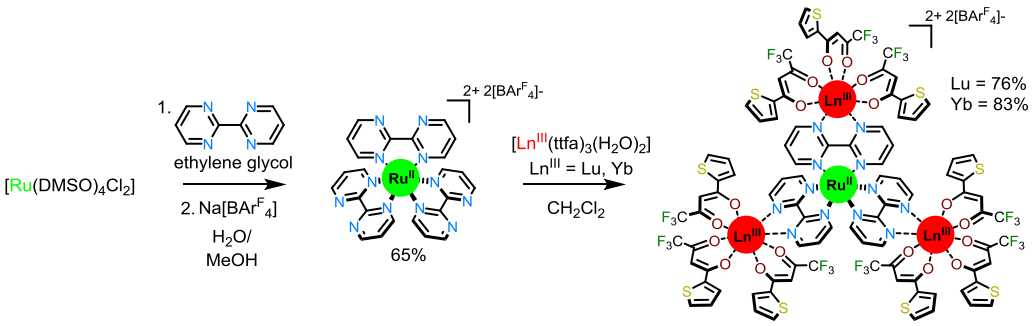

Scheme 2. Schematic representation of the synthesis of the **RuLn$_3$** heteropolynuclear complexes

Capitalizing on the success of cooperative sensitization of Tb by Yb in hetero-polynuclear clusters,[30,31] we hypothesized that hetero-polynuclear species comprising Yb complexes associated to a metal complex exhibiting an MLCT transition should be of interest to design new UC devices (**Scheme 1c**). Here, we report on the synthesis and characterization of $[(Ru(bpm)_3)(LnL_3)_3][BAr^F_4]_2$ hetero-tetranuclear *d-f* complexes (hereafter referred to as **RuLn$_3$**), in which three LnL_3 entities (Ln = Yb or Lu, L = ttfa = thenoyltrifluoroacetylacetonate) are linked to a Ru center by a bridging 2,2'-bipyrimidine (bpm) ligand[32,33] (**Scheme 2**) using a weakly coordinating $[BAr^F_4]$ (tetrakis(3,5-*bis*-trifluoromethyl)phenyl)borate) anion. A full spectroscopic analysis of the up- and downshifting energy transfer processes is presented, revealing the first example of *f*→*d* upconverting molecular device in solution.

RESULTS AND DISCUSSION

The initial $[Ru(bpm)_3][BAr^F_4]_2$ complex was prepared using a modified procedure[34] reported for the synthesis of the $[Ru(bpm)_3]Cl_2$ complex, followed by anion metathesis using $Na[BAr^F_4]$ in H_2O/MeOH (**Scheme 2**, **Figures S1-S9**).[35] Crystallization of the complex from a concentrated CH_2Cl_2 solution afforded single crystals suitable for X-ray diffraction analysis (**Figure 1**).

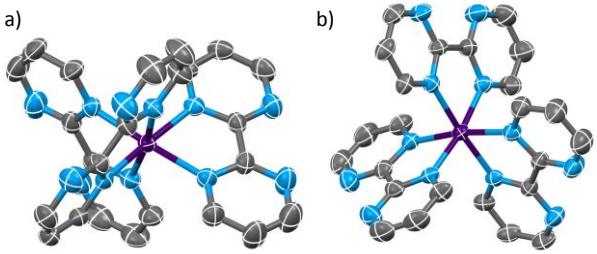

Figure 1. X-ray crystal structure of the $[Ru(bpm)_3]^{2+}$ complex along (a) and perpendicular (b) to the main pseudo-C_3 axis; ellipsoids plotted at the 50% probability level, H-atoms and counterions omitted for clarity (CCDC no. 2171569)

The solid-state structure of the complex comprises one $[Ru(bpm)_3]^{2+}$ entity together with two $[BAr^F_4]^-$ anions, lacking any significant interaction between the complex and non-coordinating counterion. The *pseudo*-octahedral $[Ru(bpm)_3]^{2+}$ core consists of κ^2 coordination of the three bpm moieties by one nitrogen atom from each of the pyrimidine rings. The mean Ru-N bond lengths are 2.07(1) Å (*cf.* 2.055 Å in the related $[Ru(bipy)_3]^{2+}$ complex[36]). In the bpm ligands, the two pyrimidine rings are almost coplanar with only 1.2(6)° between the planes of the two rings, which contrast with $[Ru(bipy)_3]^{2+}$ (mean angle of 5.9° between the rings), the latter being imparted by steric repulsion between the hydrogen atoms in the 3 and 3' positions. In order to question the distortion of the complex away from a perfect octahedron, the twist angle, ω, which defines the extent to which the two tripods formed by three N atoms related by the pseudo-C_3 axis has been rotated about the three-fold axis,[37] was measured. It amounts to 51.5(6)°, pointing to a slight distortion from the perfect octahedron (ω = 60°) towards a trigonal prismatic conformation, similarly to $[Ru(bipy)_3]^{2+}$ (ω = 51.9°).[36] Interestingly, the two *exo* nitrogen atoms of each bpm ligands point outward and are perfectly suited as bidentate ligands for bridging coordination to $LnL_3(H_2O)_2$ entities.[38–41]

In order to examine the possible coordination to form **LnL$_3$** complexes, a ^{1}H NMR titration experiment was performed in which the ^{1}H NMR spectra of a solution of $[Ru(bpm)_3]^{2+}$ were measured upon addition of increasing quantities of the diamagnetic $[LuL_3(H_2O)_2]$ complex. From **Figure 2**, one can observe the three aromatic protons of the *bpm* ligands in the *ortho*-, *meta*- and *para* position from the external coordinating nitrogen atoms (**Figure 2b**), are subject to downfield shift in the presence of increasing amounts of the Lu complex. These data suggest the gradual formation of mono-, bis- and tris-adducts of Lu with the Ru complex according to the model:

$$[Ru(bpm)_3] + YbL_3 \overset{K_1}{\leftrightarrow} [Ru(bpm)_3(YbL_3)] + YbL_3 \overset{K_2}{\leftrightarrow} [Ru(bpm)_3(YbL_3)_2] + Yb \overset{K_3}{\leftrightarrow} [Ru(bpm)_3(YbL_3)_3]$$

In which K_j represents the stepwise association constants. The shift is particularly marked for H^o, which is proximate to the coordinating Lu ion. The gradual evolution of the chemical shifts point to a rapid kinetic exchange between the different species present in solution, but considering the very smooth evolution of the chemical shifts, it was not possible to fit the data with the three successive binding constants K_1, K_2 and K_3.

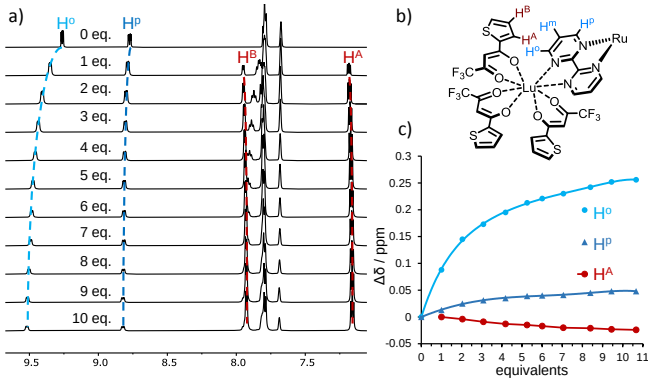

Figure 2. (a) ^{1}H NMR titration of $[Ru(bpm)_3][BAr^F]_2$ by $[LuL_3(H_2O)_2]$ in $(CD_3)_2CO$ (400 MHz, 298 K). (b) numbering

scheme. (c) evolution of the proton chemical shifts as a function of equivalents of $[LuL_3(H_2O)_2]$

Similar titration experiments were run in CD_2Cl_2 at 298 K and at 243 K, showing the same fluxional behavior (**Figure S10**, **S11**). Additionally, the incorporation of 4 Å molecular sieves at the end of the titration induced further shift of the signals, indicating a displacement of the equilibrium towards the hetero-polynuclear species upon sequestration of competitive H_2O ligands. A ^{1}H-^{1}H ROESY experiment exhibited dipolar couplings between the ortho proton H^o of the bpm ligands and H^B of the thiophene moieties, confirming the spatial proximity of LuL_3 to the bpm ligands, as expected upon complexation (**Figure S12**).

The $[Ru(bpm)_3(LnL_3)_3][BAr^F{}_4]_2$ complexes were then isolated in 76% and 83% yields for Ln = Lu and Ln = Yb respectively from combination of $[Ru(bpm)_3][BAr^F{}_4]_2$ and three equivalents of $[LnL_3(H_2O)_2]$ complexes in anhydrous CD_2Cl_2 and in the presence of molecular sieves (**Scheme 2**). The complexes were analyzed by NMR spectroscopy (**Figure S13-S15**, **S17**, **S18**), elemental analysis, infrared spectroscopy (See Electronic Supplementary Information, **Section S2.1**) and high-resolution electrospray mass spectrometry (**Figure 3**, **S16**, **S19**).

The mass spectra of the **RuYb$_3$** assemblies show monocationic peaks for the $[Ru(bpm)_3(YbL_3)_3][BAr^F{}_4]^+$ fragment, centered at *m/z* = 3947.8923 Da, in addition to characteristic peaks corresponding to the $[Ru(bpm)_3(YbL_3)][BAr^F{}_4]^+$

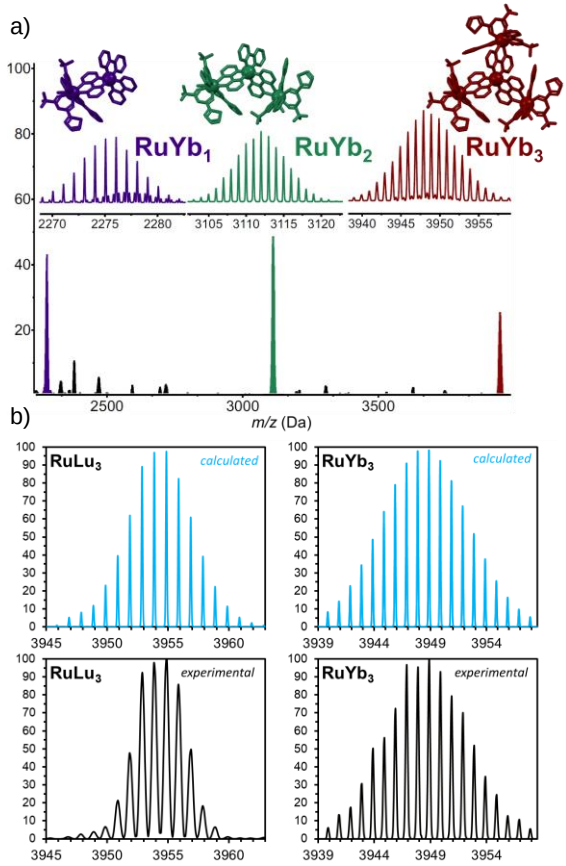

Figure 3. (a) HR-ES/MS spectrum of **RuYb$_3$** in CH_3CN with expansions of the three main peaks corresponding to $[Ru(bpm)_3(YbL_3)][BAr^F{}_4]^+$ (violet), $[Ru(bpm)_3(YbL_3)_2][BAr^F{}_4]^+$ (green) and $[Ru(bpm)_3(YbL_3)_3][BAr^F{}_4]^+$ (red) species. (b) comparison of the measured *vs.* simulated spectra for the $[Ru(bpm)_3(LnL_3)_3][BAr^F{}_4]^+$ ions (Ln = Lu (left), Yb (right)).

and $[Ru(bpm)_3(YbL_3)_2][BAr^F{}_4]^+$ complexes (**Figure 3a**). Similarly, the spectra of the **RuLu$_3$** analogue (**Figure S16**) also displayed a strong peak corresponding to the $[Ru(bpm)_3(LuL_3)_3][BAr^F{}_4]^+$ species at *m/z* = 3953.8537, together with peaks corresponding to the loss of one or two $(LuL_3)_3$ entities. Both samples gave excellent agreement of the molecular ion with the theoretical isotopic distributions (**Figure 3b**).

Considering our unsuccessful efforts to obtain the solid state structure of the heteronuclear complex by x-ray crystal diffraction, density functional theory (DFT) calculations were used to gain insight into the structural and electronic properties of $[Ru(bpm)_3]^{2+}$ and $[Ru(bpm)_3(LnL_3)_3]^{2+}$. The average Ru-N distance calculated for $[Ru(bpm)_3]^{2+}$ (2.094 Å) is in good agreement with the experimental value observed in the solid state (2.07 Å). The Ru-N coordination remains very similar in the $[Ru(bpm)_3(YbL_3)_3]^{2+}$ entity, which displays a nearly undistorted C_3 symmetry with Ru-N distances of 2.089 and 2.100 Å. The three Yb^{3+} ions define the vertices of an equilateral triangle with Yb-Yb distances (edges) of 10.88 Å and the Ru^{2+} ion placed at the center of the triangle with Ru-Yb distances of 6.28 Å (**Figure 4**).

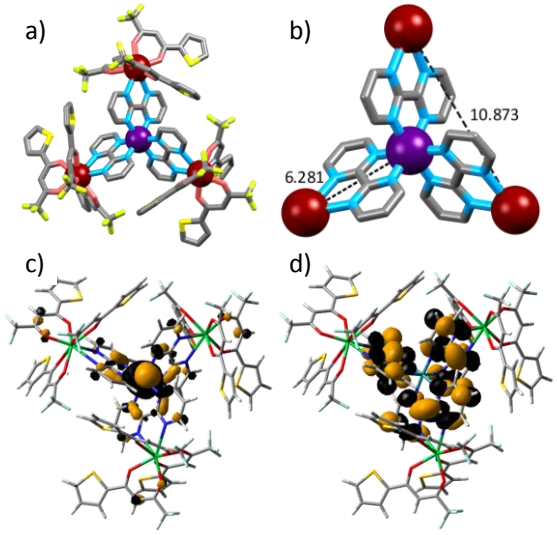

Figure 4. (a) DFT optimized geometry of the **RuYb$_3$** complex. (b) The hetero-tetrametallic core with annotated Ru-Yb and Yb-Yb bond distances (H-atoms omitted for clarity). (c) Isosurface of the HOMO-6. (d) Isosurface of the LUMO (0.02 a. u.).

The UV-Vis absorption spectrum of $[Ru(bpm)_3][BAr^F{}_4]_2$ in CH_3CN displays a strong absorption band (λ = 332 nm, ε = 13,000 M^{-1}) attributed to $\pi^* \leftarrow \pi$ transitions centered on the bpm moieties. In the visible region, a broad absorption band is observed with maximum at 454 nm (ε = 7100 M^{-1}, **Figure 5**) with a shoulder at *ca.* 420 nm, attributed to the Ru(II) to bpm ^{1}MLCT absorption. Upon excitation into this absorption at 450 nm, a broad and featureless emission band is observed, with a maximum at 635 nm. This is ascribed to the ^{3}MLCT emission band and displays a relatively modest luminescence quantum yield of 0.3%, with an excited state lifetime of 80 ns in aerated anhydrous CH_3CN solution (**Table 1**). Interestingly, one notes that the corresponding excitation spectrum does not exactly match with the absorption spectrum in this visible domain, the

high energy tail of the ^{1}MLCT band, from *ca.* 400 to 440 nm, is less efficient at sensitizing the ^{3}MLCT emission at 636 nm. Polarized emission studies on the related $[Ru(bipy)_3]^{2+}$ complex showed that the main contribution in the emission spectrum at room temperature arises from an emission polarized perpendicular to the principal C_3 axis of the molecule,[42] while absorption is comprised of two main contributions leading to two possible emitting states, strongly dependent on the temperature.[43] By analogy, one may understand the presence of two different contributions in the excitation spectrum as arising from absorption of the ^{1}MLCT polarized along and perpendicular to the main C_3 axis for the high and low energy contributions respectively.

Time-dependent density functional theory (TDDFT) calculations were used to rationalize the spectroscopic properties of $[Ru(bpm)_3]^{2+}$ with the TPSSh functional, which is shown to provide good results for Ru(II) complexes.[44] The absorption spectrum calculated for this complex matches the experimental spectrum (**Figure S22**). The 10 lowest energy excited states are responsible for the absorption at wavelengths > 400 nm, with the analysis of the MOs contributing to each absorption confirming the MLCT character of the band. Indeed, these excited states are the result of excitations from HOMO and HOMO(-1,-2) to LUMO, LUMO(+1,+2) and LUMO+3. The occupied orbitals contain a significant contribution of Ru d-orbitals (>75%, **Table S23**), while LUMO to LUMO+3 are centered on the bpm ligands (%Ru< 6%). The absorption profile at wavelengths > 440 nm is dominated by transitions to the double degenerate excited states 4 and 5 at 470 nm, which involve HOMO(-1,-2)→LUMO excitations, as well as excited states 7 and 8, which are dominated by HOMO(-1,-2)→LUMO(+1,+2) excitations. Inspection of the corresponding MOs (**Figure S24**, **Table S25**) shows that these excitations result in significant polarization perpendicular to the symmetry C_3 axis. Below 440 nm the main absorption is calculated at 418 nm (excited state 10), which is the result of a HOMO→LUMO+3 excitation. The HOMO is dominated by the contribution of a Ru 4d orbital directed along the C_3 axis, resulting in polarization along the latter. The calculated ground to excited state transition electric dipole moments support these qualitative observations (**Table S26**). The energy of the zero phonon line of the ^{3}MLCT state was estimated from the adiabatic transition energy obtained with the self-consistent field method (ΔSCF) corrected by the difference in zero-point vibrational energy of the single ground state.[45] The calculations afforded an energy of 17 288 cm^{-1} (578 nm), in excellent agreement with the value estimated from the experimental emission spectrum (17860 cm^{-1}). TDDFT calculations evidence that the ^{3}MLCT state is mainly the result of a HOMO→LUMO excitation (88%), providing a somewhat higher energy for the ^{3}MLCT state (17963 cm^{-1}, 557 nm). This is expected, as the energies provided by TDDFT are vertical, while the ΔSCF method uses the relaxed geometries of both the ground singlet state and the excited triplet state. TDDFT calculations performed for **RuYb$_3$** reveal a similar energy for the ^{3}MLCT state (17718 cm^{-1}, 564 nm), which is the result of a HOMO-6 →LUMO excitation (76%). The LUMO is located mainly on the bpm ligands (93 %), with a negligible contribution from Ru. On the contrary, HOMO-6 displays a large contribution from Ru 4d orbitals (71%), as expected considering the nature of the ^{3}MLCT state (**Figure 4c**).

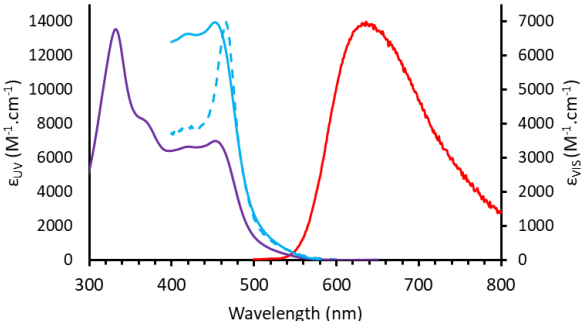

Figure 5. Absorption spectra of $[Ru(bpm)_3][BAr^F{}_4]_2$ (purple solid line, left y-axis, c = 5.6×10^{-5} M) with an expansion of the ^{1}MLCT (blue solid line, right y-axis) and normalized excitation (blue dashed line, λ_{em} = 640 nm) and emission (red solid line, λ_{exc} = 450 nm) spectra for the $[Ru(bpm)_3][BAr^F{}_4]_2$ complex in anhydrous aerated CH_3CN.

In order to investigate the degree of communication between the Ru(II) and Yb(III) moieties in the heteropolynuclear complex, a photoluminescence titration of $[Ru(bpm)_3][BAr^F{}_4]_2$ by a $[YbL_3(H_2O)_2]$ solution in anhydrous aerated CH_3CN was performed. The evolution of the emission spectra was monitored upon excitation into the ^{1}MLCT absorption band (λ_{exc} = 488 nm) and is presented in **Figure 6**. Upon titration of the ytterbium complex a decrease of the ^{3}MLCT emission band with a concomitant appearance of the characteristic Yb NIR emission arising from the $^2F_{5/2} \rightarrow {}^2F_{7/2}$ transition was observed. This is indicative of a downshifting Ru → Yb energy transfer process (**Figure S30**),[46–48] which deactivates the ^{3}MLCT state. With the intensity changes observed during the titration, the efficiency of sensitization between the Ru and the Yb ($\eta_{Ru\rightarrow Yb^*}$) was determined to be 68% using equation (3):[49]

$$\eta_{Ru\rightarrow Yb} = 1 - \frac{\int I_{RuYb}(\lambda_E,\lambda_F)d\lambda_F}{\int I_{Ru}(\lambda_E,\lambda_F)d\lambda_F} \qquad (3)$$

In which the upper and lower part of the right term are the integrated emission of Ru (measured from 500 to 900 nm) in presence and absence of Yb, respectively, assuming that the emission intensity at the end of the titration was that of the **RuYb$_3$** species. This sensitization efficiency of 68% is considerably higher than other previously reported bimetallic Ru-Yb arrays (*ca.* 10%),[33,46] with the presence of multiple Yb energy acceptors and the short Ru-Yb internuclear distance being a likely explanation.

Importantly, the Ru to Yb energy transfer efficiency is also related to the excited state lifetimes of the Ru in presence (τ_{RuYb3}) and in absence (τ_{Ru}) of the Yb acceptor by the relationship:

$$\eta_{Ru\rightarrow Yb} = 1 - \frac{\tau_{RuYb3}}{\tau_{Ru}} \qquad (4)$$

In this way, the excited state lifetime of Ru in the **RuYb$_3$** complex can be estimated to be 26 ns, a lifetime that we could unfortunately not verify experimentally, due to the high concentration and optical density of the complex mandatory for its stability in solution.

	ε_{ligand} /10^4 $M^{-1}.cm^{-1}$ (λ/nm)	ε_{MLCT} $M^{-1}.cm^{-1}$ (λ/nm)	ε_{Yb} $M^{-1}.cm^{-1}$	τ_{Yb} µs[a]	τ_{radYb} µs	τ_{Ru} ta	Φ_{UC}[b] (×10^{-8})
$[Ru(bpm)_3]^{2+}$	1.3 (332)	7100 (454)	-	-	-	80	-
RuYb$_3$	8.7 (267)	6500 (453)	21	16	681		2.1

		976 nm
RuLu$_3$	10.0 (266)	7200 (453)

Table 1. Photophysical properties of the different complexes obtained in anhydrous aerated CH_3CN at 298 K. [a] Excitation at 455 nm using a NanoLed-455 from Horiba Jobin Yvon Fluorolog. [b] Excitation at 980 nm (P = 6.9 W/cm^2), using $[Ru(bipy)_3Cl_2]$ in water (Φ = 0.04; λ_{exc} = 450 nm) as reference for the calculation of the UC quantum yield.[50]

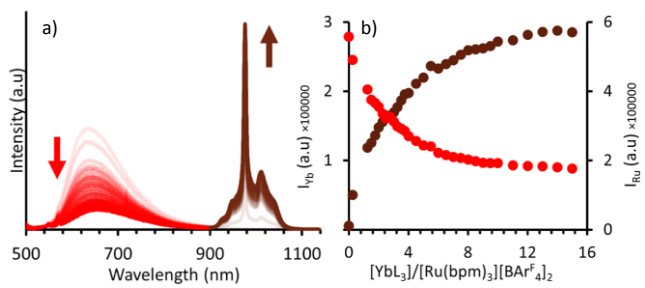

Figure 6. (a) Emission spectra of the Yb and the ^{3}MLCT of Ru during the titration of $[Ru(bpm)_3][BAr^F_4]_2$ (1.23×10^{-4} M) by successive addition of a solution of $[YbL_3(H_2O)_2]$ (4.98 mM, anhydrous CH_3CN). (b) Evolution of the emission integral of the Yb (dark red) and the ^{3}MLCT of the Ru (red) (λ_{exc}= 488 nm).

Having investigated the spectroscopy of the *in situ* formed **RuLn$_3$** edifice, the photophysical characterization of the isolated **RuLn$_3$** complexes was performed (**Figure 7**, **Figure S31**). The **RuYb$_3$** complexes broadly retains the properties of the parent $[Ru(bpm)_3][BAr^F_4]_2$ complex. The UV absorption bands at 337 nm (ε = 180,000 M^{-1}) are significantly more intense owing to the overlap of the π*←π transitions centered on the *bpm* moieties and the π*← π ones of the L ligands.[51] The ^{1}MLCT absorption centered around 453 nm (ε = 6,500 M^{-1}) is largely unperturbed upon Yb complexation. This is borne out for the ^{3}MLCT excitation and emission spectra (λ_{em} = 636 nm). Once again significant emission from the Yb(III) $^2F_{5/2} \rightarrow {}^2F_{7/2}$ transition (λ_{em} = 977 nm) is achieved *via* excitation of the ruthenium absorption band (λ_{exc} = 450 nm), with an excited state lifetime for Yb of 16 µs. The overly large optical density of the sample, required to preclude dissociation of the complex at low concentrations, impeded the measurement of the Ru excited state lifetime (ns range) with our setup. However, this can also be estimated to be 26 ns according to the titration.

From the NIR absorption spectra recorded for **RuYb$_3$** (**Figure 7**), the methodology of Werts and coworkers[52] was applied to determine the radiative lifetime of Yb in the complex using equation (5):

$$\frac{1}{\tau_{rad}} = 2303 * \frac{8\pi c n^2 \tilde{\upsilon}^2}{N_A} \frac{g_l}{g_u} \int \varepsilon(\tilde{\upsilon}) d\,\tilde{\upsilon} \qquad (5)$$

$$\tilde{\upsilon} = \frac{\int \tilde{\upsilon} \times \varepsilon(\tilde{\upsilon}) d\tilde{\upsilon}}{\int \varepsilon(\tilde{\upsilon}) d\tilde{\upsilon}} \qquad (6)$$

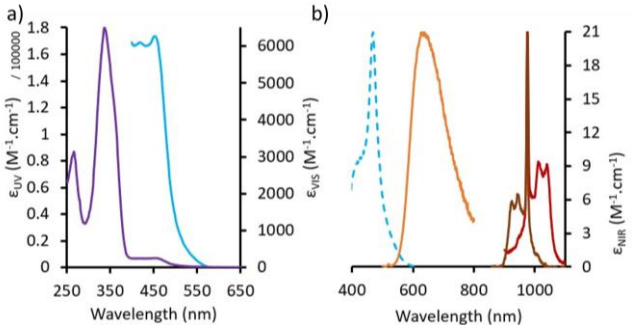

Figure 7. (a) Absorption spectra of the complex (purple solid line, left y-axis) with an expansion of the ^{1}MLCT absorption (blue solid line, right y-axis, c = 5.7×10^{-6} M). (b) Absorption spectrum of Yb in the NIR (brown, c = 1.81 mM), normalized excitation spectrum (blue dashed line – λ_{em} = 640 nm), and emission spectra of Ru in the NIR/visible (orange – λ_{exc} = 450 nm) and Yb (dark red, λ_{exc} = 450 nm) spectra for the $[Ru(bpm)_3(YbL_3)_3][BAr^F_4]_2$ complex in anhydrous CH_3CN.

In which N_A is Avogadro's number, $\tilde{\upsilon}$ is the barycentre of the transition (cm^{-1}), c is the speed of light in vacuum (cm.s^{-1}), n is the refractive index of the medium (n_{CH3CN} = 1.33), $\varepsilon(\tilde{\upsilon})$ is the absorption spectrum of the transition (M^{-1}.cm^{-1}), g_l and g_u are related to the degeneracies of the ground and excited states, respectively, and are equal to $2J+1$ where J = 7/2 for g_l and J = 5/2 for g_u. A radiative lifetime of 681 µs was determined for Yb in the **RuYb$_3$** complex. The Yb centered luminescence quantum yield, Φ_{Yb}^{Yb}, could then be calculated to be 2.3% using equation (7):

$$\Phi_{Yb}^{Yb} = \frac{\tau_{obs}}{\tau_{rad}} \qquad (7)$$

Finally, the overall quantum yield for emission of Yb upon excitation of Ru in the ^{1}MLCT absorption band $\Phi_{Ov.}$ was calculated to be 1.6% with equation (8):

$$\Phi_{Ov.} = \eta_{Ru \rightarrow Yb^{*\times}} \Phi_{Yb}^{Yb} \qquad (8)$$

Unfortunately, it was not possible to determine $\Phi_{Ov.}$ by direct methods, the high optical density of the sample precluding its determination comparing with standard references.

The most striking observation in the photophysical characterization of the **RuYb$_3$** assembly arises from upconversion experiments *via* direct excitation of the ytterbium ions. Upon excitation at 980 nm into the Yb $^2F_{5/2} \leftarrow {}^2F_{7/2}$ absorption band a broad structureless band is observed at 636 nm, characteristic of the ruthenium ^{3}MLCT emissive state (**Figure 8a**)

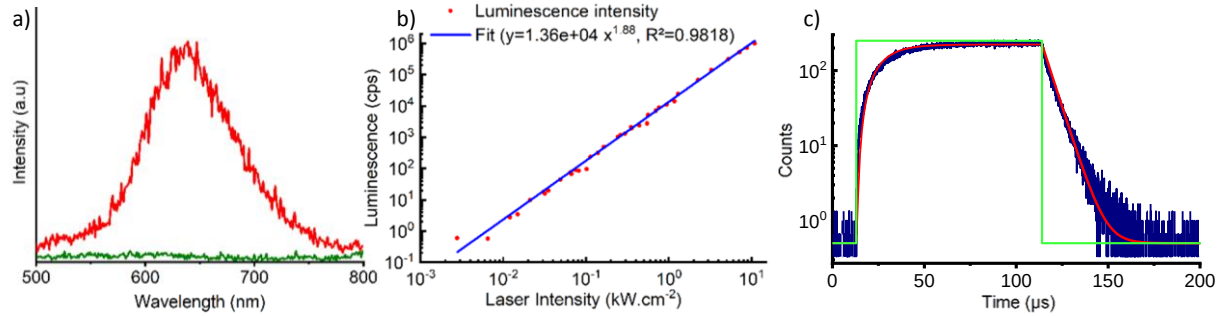

Figure 8. (a) UC emission of the $[Ru(bpm)_3(YbL_3)_3][BAr^F{}_4]_2$ (red – 0.39 mM) and $[Ru(bpm)_3(LuL_3)_3][BAr^F{}_4]_2$ (green – 0.39 mM) complexes in aerated anhydrous CH_3CN (λ_{exc} = 980 nm, P = 6.9 W/cm²). (b) UC intensity as a function of the incident pump intensity in a Log/Log scale for $[Ru(bpm)_3(YbL_3)_3][BAr^F{}_4]_2$. (c) Time-resolved rise and decay curves of the UC emission at 630±37 nm upon time-gated excitation at 974 nm (8.1 kW.cm^{-2} (green line)) for a 1.3 mM solution of $[Ru(bpm)_3(YbL_3)_3][BAr^F{}_4]_2$. The red line corresponds to the fit of the data and the green line to the periods during which the laser was turned on and off.

Crucially this emission was absent for the spectroscopically silent **RuLu$_3$** complex, implicating Yb as an energy relay in the UC process. Investigating the dependency of the emission on the incident laser intensity in the form of a Log/Log plot gives a linear response with a slop of 1.88 indicative of a two-photon process (**Figure 8b**).[53]

We also investigated the time-resolved evolution of the UC signal using pulsed excitation during which the laser irradiates for a 100 µs period over 200 µs (**Figure 8c**, green line). As can be evidenced on the **Figure 8c**, the UC signal slowly rises to a quasi steady-state regime within the 100 µs period and rapidly decayed once the laser was switched off. Interestingly, the slow rise is only weakly affected by the excitation power density of the laser from 0.3 to 10.9 KW.cm^{-2} (**Figure S35**), indicating that a slow kinetic step is implicated in the UC emission. Regarding the decay observed after the laser was switch off, it appeared to be extremely long lived compared to <100 ns observed for the Ru lifetimes measured upon excitation into the ^{1}MLCT absorption band. This apparent long-lived emission is associated to a slow feeding of the Ru centered excited state, as can be found in *e.g.* delayed luminescence. To account for these different observations, we propose the energy level diagram depicted in **Figure 9**. The UC quantum yield was determined according to a previously published procedure[4] to 2.1×10^{-8} at P = 6.9 W/cm².

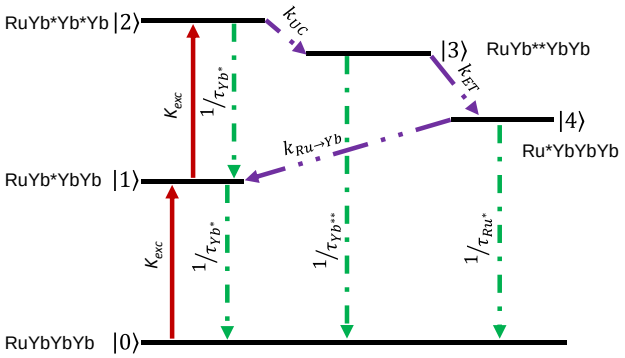

Figure 9. Energy level diagram of the *d-f* cooperative sensitization UC mechanism in **RuYb$_3$**.

In the first step, a photon is absorbed by the ground state to form a $RuYb^*Yb_2$ species, with one Yb in its excited state. A second photon is then absorbed by a second Yb ion to lead to the formation of the doubly excited state RuYb*Yb*Yb. A slow recombination step occurs by cooperative sensitization to obtain a doubly excited Yb** ion in a $RuYb^{**}Yb_2$ species, as previously observed in nonanuclear Yb clusters.[30] Either this species emits photons, leading to a cooperative luminescence process (not observed), with an excited state lifetime denoted $\tau_{Yb^{**}}$, or, the energy is transferred to the Ru MLCT state to form the Ru^*Yb_3 excited state, leading to the observed Ru emission, with a lifetime of 26 ns (*vide supra*). To account for the previous observation of Yb emission upon Ru excitation, back-transfer to an Yb ion is added in the overall diagram. The rate transfer of this step, $k_{Ru\rightarrow Yb}$, can be estimated from the lifetimes of the free Ru complex and that of the $RuYb_3$ species by the equation:

$$k_{Ru\rightarrow Yb} = \frac{1}{\tau_{RuYb3}} - \frac{1}{\tau_{Ru}} \qquad (9)$$

Affording a value of 26×10^6 s^{-1} for $k_{Ru\rightarrow Yb}$. From this diagram, the populations of the different states, denoted $|0\rangle$ to $|4\rangle$, can be modeled with the following matrix:

$$\frac{d}{dt}\begin{pmatrix}|0\rangle\\|1\rangle\\|2\rangle\\|3\rangle\\|4\rangle\end{pmatrix} = \begin{pmatrix} -3k_{exc} & k_{Yb^*} & 0 & k_{Yb^{**}} & k_{Ru} \\ 3k_{exc} & -2k_{exc}-k_{Yb^*} & 2k_{Yb^*} & 0 & k_{Ru\rightarrow Yb} \\ 0 & 2k_{exc} & -2k_{Yb^*}-k_{UC} & 0 & 0 \\ 0 & 0 & k_{UC} & -k_{Yb^{**}}-k_{ET} & 0 \\ 0 & 0 & 0 & -k_{ET} & -k_{Ru}-k_{Ru\rightarrow Yb} \end{pmatrix} \times \begin{pmatrix}|0\rangle\\|1\rangle\\|2\rangle\\|3\rangle\\|4\rangle\end{pmatrix}$$

In which k_{exc} is the pumping rate constant defined by:

$$k_{exc} = \frac{\lambda_P}{hc} P \sigma_{Yb}^{0\rightarrow 1} \qquad (10)$$

λ_P being the pumping wavelength, c the speed of light in vacuum, h is Planck's constant, P the incident pump intensity and $\sigma_{Yb}^{0\rightarrow 1}$ the absorption cross section of Yb (in cm²/molecule). The temporal evolution of the Ru based UC emission observed upon Yb excitation at 974 nm (**Figure 8c**) was then fitted according to the proposed model in two steps, first fitting the rise of the signal ($k_{exc} \neq 0$), then fitting the decay (k_{exc} = 0) keeping $k_{Yb^*} = 1/\tau_{Yb^*} = 58\times10^3$ s^{-1}, $k_{Ru\rightarrow Yb} = 26\times10^6$ s^{-1} and $k_{Ru^*} = 1/\tau_{Ru^*} = 38.5\times10^6$ s^{-1} as constants in the fitting. Full experimental details on the fitting procedure are given in the supplementary information.

The best fitting (**Figure 8c**, **Figure S36-S39**) was obtained for values of $k_{UC} = 60\times10^3$ s^{-1} , $k_{Yb^{**}} = 640\times10^3$ s^{-1} , corresponding to an excited state lifetime of 1.6 µs for Yb**, and $k_{ET} = 7.6\times10^6$ s^{-1}. One notes that the rate leading to the cooperative upconversion phenomenon, k_{UC}, is far slower than all of the other steps and is rate determining in the process, which explains the slow rise of the UC signal. In contrast, the energy transfer from Yb** to the Ru centered excited state, k_{ET}, is very fast, explaining the absence of luminescence from the cooperative UC, and only observation of emission from the ^{3}MLCT state. Finally, the excited state lifetime of the "virtual" Yb** state is shorter than that of Yb*, but not in the range of one half, as proposed by some authors for cooperative luminescence in solids.[54] It should be emphasized that the value of k_{UC} is approximately 25 times larger than that previously observed in heteropolynuclear Yb/Tb complexes displaying cooperative photosensitization (2330 s^{-1}),[4] demonstrating the utility in using a spin-allowed MLCT absorption as an acceptor for UC.

CONCLUSION

We have prepared a novel hetero-tetrametallic supramolecular assembly between a $[Ru(bpm)_3]^{2+}$ core and LnL_3 fragments to yield complexes of the general formula $[Ru(bpm)_3(LnL_3)_3][BAr^F{}_4]_2$ (Ln = Lu, Yb). The parent $[Ru(bpm)_3][BAr^F{}_4]_2$ complex exhibits slightly distorted C_3 symmetry with minimal interplanar distortion of the bpm rings (NCCN dihedral = 1.2(6)°). ^{1}H NMR investigations in acetone-d^6 reveal a weak coordination of the LuL_3 fragment

with the peripheral bipyrimidine nitrogen atoms, which could be enhanced by switching to non-coordinating CD_2Cl_2 under anhydrous conditions. A dipolar through-space NOE experiment indicated the assembly of the four components, which was supported by mass spectrometry showing characteristic peaks corresponding to **RuLn$_1$**, **RuLn$_2$**, and **RuLn$_3$** species. For the Yb variant, photoluminescence titrations revealed downshifting energy transfer from the $[Ru(bpm)_3]^{2+}$ core to the outer YbL_3 entities. Upon excitation of the ^{1}MLCT absorption band an emission band attributed to the $^2F_{5/2} \rightarrow {}^2F_{7/2}$ electronic transition of Yb was observed at 976 nm, with a sensitization efficiency of 68%. Upconversion experiments reveal that excitation of the Yb $^2F_{5/2} \leftarrow {}^2F_{7/2}$ absorption band engenders emission of the ^{3}MLCT state of the $[Ru(bpm)_3]^{2+}$ core at 636 nm with an UCQY of 2.1×10^{-8}. Log/Log experiments confirmed the quadratic dependence of the UC emission *vs.* the power of the excitation, and kinetic experiments reveal a relatively long rise of the emission which could be modeled according to a cooperative sensitization mechanism. This represents the first example of an *f→d* upconverting molecular device and opens many opportunities for even more efficient devices using a combination of *d*- and *f*-elements.

ASSOCIATED CONTENT

This material is available free of charge via the Internet at http://pubs.acs.org.

AUTHOR INFORMATION

Corresponding Author

* **Loïc J. Charbonnière** - Equipe de Synthèse Pour l'Analyse (SynPA), Institut Pluridisciplinaire Hubert Curien (IPHC), UMR 7178, CNRS, Université de Strasbourg, ECPM, 25 rue Becquerel, 67087, Strasbourg Cedex, France. E-mail: l.charbonn@unistra.fr

* **Richard C. Knighton** - Equipe de Synthèse Pour l'Analyse (SynPA), Institut Pluridisciplinaire Hubert Curien (IPHC), UMR 7178, CNRS, Université de Strasbourg, ECPM, 25 rue Becquerel, 67087, Strasbourg Cedex, France. E-mail: knighton@unistra.fr

Present Addresses

Lohona K. Soro - Equipe de Synthèse Pour l'Analyse (SynPA), Institut Pluridisciplinaire Hubert Curien (IPHC), UMR 7178, CNRS, Université de Strasbourg, ECPM, 25 rue Becquerel, 67087, Strasbourg Cedex, France.

Waygen Thor - Equipe de Synthèse Pour l'Analyse (SynPA), Institut Pluridisciplinaire Hubert Curien (IPHC), UMR 7178, CNRS, Université de Strasbourg, ECPM, 25 rue Becquerel, 67087, Strasbourg Cedex, France. Department of Chemistry, Hong Kong Baptist University, Kowloon Tong, Kowloon, Hong Kong SAR (China).

Jean-Marc Strub - Laboratoire de Spectrometrie de Masse Bio-Organique, IPHC, UMR 7178, CNRS-Université de Strasbourg, ECPM, 25, rue Becquerel, 67087 Strasbourg, France.

Sarah Cianférani - Laboratoire de Spectrometrie de Masse Bio-Organique, IPHC, UMR 7178, CNRS-Université de Strasbourg, ECPM, 25, rue Becquerel, 67087 Strasbourg, France.

Marc Lenertz - Institut de Physique et Chimie des Matériaux de Strasbourg (IPCMS), UMR 7504, CNRS/Université de Strasbourg, 23 rue du Lœss, BP 43, 67034 Strasbourg Cedex 2, France.

Ka-Leung Wong - Department of Chemistry, Hong Kong Baptist University, Kowloon Tong, Kowloon, Hong Kong SAR (China).

Carlos Platas-Iglesias - Centro de Investigacións Científicas Avanzadas (CICA) and Departamento de Química, Universidade da Coruña, Campus da Zapateira-Rúa da Fraga 10, 15008 A Coruña, Spain.

Frédéric Przybilla - Laboratoire de Bioimagerie et Pathologies, CNRS UMR 7021, Faculté de Pharmacie CS60024 74, Route du Rhin, 67401 Illkirch-Graffenstaden, France.

ACKNOWLEDGMENT

Financial support is gratefully acknowledged (LJC and RCK) from the French Ministère de l'Education Nationale et de la Recherche, the French Canada Research Fund (LKS), Frontier Research in Chemistry Foundation (LabEx CSC, ANR-10-LABX-0026_CSC), and the French National research agency (LAPIN project n° ANR-20-CE09-0021-02; LUCAS project n°ANR-19-CE29-0014-01) for financial support. CPI thanks the Centro de Computación de Galicia (CESGA) for providing the computer facilities and the Ministerio de Ciencia e Innovación (Grant PID2019-104626GB-I00).

REFERENCES

(1) Auzel, F. Upconversion Processes in Coupled Ion Systems. *J. Lumin.* **1990**, *45* (1), 341–345. https://doi.org/10.1016/0022-2313(90)90189-I.

(2) Gamelin, D. R.; Güdel, H. U. Design of Luminescent Inorganic Materials: New Photophysical Processes Studied by Optical Spectroscopy. *Acc. Chem. Res.* **2000**, *33* (4), 235–242. https://doi.org/10.1021/ar990102y.

(3) Golesorkhi, B.; Nozary, H.; Fürstenberg, A.; Piguet, C. Erbium Complexes as Pioneers for Implementing Linear Light-Upconversion in Molecules. *Mater. Horiz.* **2020**, *7* (5), 1279–1296. https://doi.org/10.1039/C9MH01899A.

(4) Nonat, A.; Bahamyirou, S.; Lecointre, A.; Przybilla, F.; Mély, Y.; Platas-Iglesias, C.; Camerel, F.; Jeannin, O.; Charbonnière, L. J. Molecular Upconversion in Water in Heteropolynuclear Supramolecular Tb/Yb Assemblies. *J. Am. Chem. Soc.* **2019**, *141* (4), 1568–1576. https://doi.org/10.1021/jacs.8b10932.

(5) Aboshyan-Sorgho, L.; Besnard, C.; Pattison, P.; Kittilstved, K. R.; Aebischer, A.; Bünzli, J.-C. G.; Hauser, A.; Piguet, C. Near-Infrared→Visible Light Upconversion in a Molecular Trinuclear d–f–d Complex. *Angew. Chem. Int. Ed.* **2011**, *50* (18), 4108–4112. https://doi.org/10.1002/anie.201100095.

(6) Souri, N.; Tian, P.; Platas-Iglesias, C.; Wong, K.-L.; Nonat, A.; Charbonnière, L. J. Upconverted Photosensitization of Tb Visible Emission by NIR Yb Excitation in Discrete Supramolecular Heteropolynuclear Complexes. *J. Am. Chem. Soc.* **2017**, *139* (4), 1456–1459. https://doi.org/10.1021/jacs.6b12940.

(7) Golesorkhi, B.; Fürstenberg, A.; Nozary, H.; Piguet, C. Deciphering and Quantifying Linear Light Upconversion in Molecular Erbium Complexes. *Chem. Sci.* **2019**, *10* (28), 6876–6885. https://doi.org/10.1039/C9SC02068C.

(8) Soro, L. K.; Charpentier, C.; Przybilla, F.; Mély, Y.; Nonat, A. M.; Charbonnière, L. J. Yb to Tb Cooperative Upconversion in Supramolecularly Assembled Complexes in a Solution. *Chemistry* **2021**, *3* (3), 1037–1046. https://doi.org/10.3390/chemistry3030074.

(9) Aboshyan-Sorgho, L.; Cantuel, M.; Petoud, S.; Hauser, A.; Piguet, C. Optical Sensitization and Upconversion in Discrete Polynuclear Chromium–Lanthanide Complexes. *Coord. Chem. Rev.* **2012**, *256* (15), 1644–1663. https://doi.org/10.1016/j.ccr.2011.12.013.

(10) Nonat, A.; Chan, C. F.; Liu, T.; Platas-Iglesias, C.; Liu, Z.; Wong, W.-T.; Wong, W.-K.; Wong, K.-L.; Charbonnière, L. J. Room Temperature Molecular up Conversion in Solution. *Nat. Commun.* **2016**, *7* (1), 11978. https://doi.org/10.1038/ncomms11978.

(11) Roy, I.; Garci, A.; Beldjoudi, Y.; Young, R. M.; Pe, D. J.; Nguyen, M. T.; Das, P. J.; Wasielewski, M. R.; Stoddart, J. F. Host–

Guest Complexation-Mediated Supramolecular Photon Upconversion. *J. Am. Chem. Soc.* **2020**, *142* (39), 16600–16609. https://doi.org/10.1021/jacs.0c05445.

(12) Hyppänen, I.; Lahtinen, S.; Ääritalo, T.; Mäkelä, J.; Kankare, J.; Soukka, T. Photon Upconversion in a Molecular Lanthanide Complex in Anhydrous Solution at Room Temperature. *ACS Photonics* **2014**, *1* (5), 394–397. https://doi.org/10.1021/ph500047j.

(13) Golesorkhi, B.; Naseri, S.; Guénée, L.; Taarit, I.; Alves, F.; Nozary, H.; Piguet, C. Ligand-Sensitized Near-Infrared to Visible Linear Light Upconversion in a Discrete Molecular Erbium Complex. *J. Am. Chem. Soc.* **2021**, *143* (37), 15326–15334. https://doi.org/10.1021/jacs.1c06865.

(14) Gálico, D. A.; Ovens, J. S.; Sigoli, F. A.; Murugesu, M. Room-Temperature Upconversion in a Nanosized {Ln15} Molecular Cluster-Aggregate. *ACS Nano* **2021**, *15* (3), 5580–5585. https://doi.org/10.1021/acsnano.1c00580.

(15) Wang, J.; Jiang, Y.; Liu, J.-Y.; Xu, H.-B.; Zhang, Y.-X.; Peng, X.; Kurmoo, M.; Ng, S. W.; Zeng, M.-H. Discrete Heteropolynuclear Yb/Er Assemblies: Switching on Molecular Upconversion Under Mild Conditions. *Angew. Chem. Int. Ed.* **2021**, *60* (41), 22368–22375. https://doi.org/10.1002/anie.202107637.

(16) Monteiro, J. H. S. K.; Hiti, E. A.; Hardy, E. E.; Wilkinson, G. R.; Gorden, J. D.; Gorden, A. E. V.; de Bettencourt-Dias, A. New Up-Conversion Luminescence in Molecular Cyano-Substituted Naphthylsalophen Lanthanide(Iii) Complexes. *Chem Commun* **2021**, *57* (20), 2551–2554. https://doi.org/10.1039/D0CC08128K.

(17) Kalmbach, J.; Wang, C.; You, Y.; Förster, C.; Schubert, H.; Heinze, K.; Resch-Genger, U.; Seitz, M. Near-IR to Near-IR Upconversion Luminescence in Molecular Chromium Ytterbium Salts. *Angew. Chem. Int. Ed.* **2020**, *59* (42), 18804–18808. https://doi.org/10.1002/anie.202007200.

(18) Kiseleva, N.; Nazari, P.; Dee, C.; Busko, D.; Richards, B. S.; Seitz, M.; Howard, I. A.; Turshatov, A. Lanthanide Sensitizers for Large Anti-Stokes Shift Near-Infrared-to-Visible Triplet–Triplet Annihilation Photon Upconversion. *J. Phys. Chem. Lett.* **2020**, *11* (7), 2477–2481. https://doi.org/10.1021/acs.jpclett.0c00221.

(19) Bünzli, J.-C. G.; Piguet, C. Taking Advantage of Luminescent Lanthanide Ions. *Chem. Soc. Rev.* **2005**, *34* (12), 1048–1077. https://doi.org/10.1039/B406082M.

(20) Pucci, D.; Bellusci, A.; Crispini, A.; Ghedini, M.; Godbert, N.; Szerb, E. I.; Talarico, A. M. Room Temperature Columnar Mesomorphism and High Quantum Yield Phosphorescence in Ionic Ruthenium(Ii) 2,2′-Bipyridine-Based Complexes. *J. Mater. Chem.* **2009**, *19* (41), 7643–7649. https://doi.org/10.1039/B911017H.

(21) You, Y.; Park, S. Y. Phosphorescent Iridium(Iii) Complexes: Toward High Phosphorescence Quantum Efficiency through Ligand Control. *Dalton Trans.* **2009**, No. 8, 1267–1282. https://doi.org/10.1039/B812281D.

(22) Lai, P.-N.; Brysacz, C. H.; Alam, M. K.; Ayoub, N. A.; Gray, T. G.; Bao, J.; Teets, T. S. Highly Efficient Red-Emitting Bis-Cyclometalated Iridium Complexes. *J. Am. Chem. Soc.* **2018**, *140* (32), 10198–10207. https://doi.org/10.1021/jacs.8b04841.

(23) Williams, J. A. G.; Beeby, A.; Davies, E. S.; Weinstein, J. A.; Wilson, C. An Alternative Route to Highly Luminescent Platinum(II) Complexes: Cyclometalation with N/\C/\N-Coordinating Dipyridylbenzene Ligands. *Inorg. Chem.* **2003**, *42* (26), 8609–8611. https://doi.org/10.1021/ic035083+.

(24) Zhu, J.-L.; Xu, L.; Ren, Y.-Y.; Zhang, Y.; Liu, X.; Yin, G.-Q.; Sun, B.; Cao, X.; Chen, Z.; Zhao, X.-L.; Tan, H.; Chen, J.; Li, X.; Yang, H.-B. Switchable Organoplatinum Metallacycles with High Quantum Yields and Tunable Fluorescence Wavelengths. *Nat. Commun.* **2019**, *10* (1), 4285. https://doi.org/10.1038/s41467-019-12204-7.

(25) Twilton, J.; Le, C. (Chip); Zhang, P.; Shaw, M. H.; Evans, R. W.; MacMillan, D. W. C. The Merger of Transition Metal and Photocatalysis. *Nat. Rev. Chem.* **2017**, *1* (7), 0052. https://doi.org/10.1038/s41570-017-0052.

(26) Nakamaru, K. Synthesis, Luminescence Quantum Yields, and Lifetimes of Trischelated Ruthenium(II) Mixed-Ligand Complexes Including 3,3′-Dimethyl-2,2′-Bipyridyl. *Bull. Chem. Soc. Jpn.* **1982**, *55* (9), 2697–2705. https://doi.org/10.1246/bcsj.55.2697.

(27) Tanner, P. A.; Zhou, L.; Duan, C.; Wong, K.-L. Misconceptions in Electronic Energy Transfer: Bridging the Gap between Chemistry and Physics. *Chem. Soc. Rev.* **2018**, *47* (14), 5234–5265. https://doi.org/10.1039/C8CS00002F.

(28) Bergstrand, J.; Liu, Q.; Huang, B.; Peng, X.; Würth, C.; Resch-Genger, U.; Zhan, Q.; Widengren, J.; Ågren, H.; Liu, H. On the Decay Time of Upconversion Luminescence. *Nanoscale* **2019**, *11* (11), 4959–4969. https://doi.org/10.1039/C8NR10332A.

(29) Schaudel, B.; Goldner, P.; Prassas, M.; Auzel, F. Cooperative Luminescence as a Probe of Clustering in Yb3+ Doped Glasses. *J. Alloys Compd.* **2000**, *300–301*, 443–449. https://doi.org/10.1016/S0925-8388(99)00760-4.

(30) Knighton, R. C.; Soro, L. K.; Francés-Soriano, L.; Rodríguez-Rodríguez, A.; Pilet, G.; Lenertz, M.; Platas-Iglesias, C.; Hildebrandt, N.; Charbonnière, L. J. Cooperative Luminescence and Cooperative Sensitisation Upconversion of Lanthanide Complexes in Solution. *Angew. Chem. Int. Ed.* **2022**, *61* (4), e202113114. https://doi.org/10.1002/anie.202113114.

(31) Knighton, R.; Soro, L. K.; Lecointre, A.; Pilet, G.; Fateeva, A.; laurie pontille; Francés-Soriano, L. L.; Hildebrandt, N.; Charbonnière, L. J. Upconversion in Molecular Hetero-Nonanuclear Lanthanide Clusters in Solution. **2020**. https://doi.org/10.26434/chemrxiv.13193741.v1.

(32) Zabierowski, P. W.; Jeannin, O.; Fix, T.; Guillemoles, J.-F.; Charbonnière, L. J.; Nonat, A. M. From Mono- to Polynuclear Coordination Complexes with a 2,2′-Bipyrimidine-4,4′-Dicarboxylate Ligand. *Inorg. Chem.* **2021**, *60* (11), 8304–8314. https://doi.org/10.1021/acs.inorgchem.1c00938.

(33) Lazarides, T.; Adams, H.; Sykes, D.; Faulkner, S.; Calogero, G.; Ward, M. D. Heteronuclear Bipyrimidine-Bridged Ru–Ln and Os–Ln Dyads: Low-Energy 3MLCT States as Energy-Donors to Yb(Iii) and Nd(Iii). *Dalton Trans.* **2008**, No. 5, 691–698. https://doi.org/10.1039/B714640J.

(34) Hunziker, M.; Ludi, A. Ruthenium(II)-Bipyrimidine Complexes. Spectroscopic and Electrochemical Properties of a Novel Series of Compounds. *J. Am. Chem. Soc.* **1977**, *99* (22), 7370–7371. https://doi.org/10.1021/ja00464a054.

(35) Lin, S.; Ischay, M. A.; Fry, C. G.; Yoon, T. P. Radical Cation Diels–Alder Cycloadditions by Visible Light Photocatalysis. *J. Am. Chem. Soc.* **2011**, *133* (48), 19350–19353. https://doi.org/10.1021/ja2093579.

(36) Rillema, D. P.; Jones, D. S. Structure of Tris(2,2′-Bipyridyl)Ruthenium(II) Hexafluorophosphate, [Ru(Bipy)3][PF6]2; X-Ray Crystallographic Determination. *J. Chem. Soc. Chem. Commun.* **1979**, No. 19, 849–851. https://doi.org/10.1039/C39790000849.

(37) Charbonnière, L. J.; Williams, A. F.; Piguet, C.; Bernardinelli, G.; Rivara-Minten, E. Structural, Magnetic, and Electrochemical Properties of Dinuclear Triple Helices: Comparison with Their Mononuclear Analogues. *Chem. – Eur. J.* **1998**, *4* (3), 485–493. https://doi.org/10.1002/(SICI)1521-3765(19980310)4:3<485::AID-CHEM485>3.0.CO;2-8.

(38) Fernandes, J. A.; Sá Ferreira, R. A.; Pillinger, M.; Carlos, L. D.; Jepsen, J.; Hazell, A.; Ribeiro-Claro, P.; Gonçalves, I. S. Investigation of Europium(III) and Gadolinium(III) Complexes with Naphthoyltrifluoroacetone and Bidentate Heterocyclic Amines. *J. Lumin.* **2005**, *113* (1), 50–63. https://doi.org/10.1016/j.jlumin.2004.08.052.

(39) Irfanullah, M.; Iftikhar, K. New Dinuclear Lanthanide(III) Complexes Based on 6,6,7,7,8,8,8-Heptafluoro-2,2-Dimethyl-3,5-Octanedione and 2,2′-Bipyrimidine. *Inorg. Chem. Commun. - INORG CHEM COMMUN* **2009**, *12*, 296–299. https://doi.org/10.1016/j.inoche.2009.01.007.

(40) Kadjane, P.; Charbonnière, L.; Camerel, F.; Lainé, P. P.; Ziessel, R. Improving Visible Light Sensitization of Luminescent Europium Complexes. *J. Fluoresc.* **2008**, *18* (1), 119–129. https://doi.org/10.1007/s10895-007-0250-9.

(41) Ilmi, R.; Iftikhar, K. Optical Emission Studies of New Europium and Terbium Dinuclear Complexes with Trifluoroacetylacetone and Bridging Bipyrimidine. Fast Radiation and High Emission Quantum Yield. *Polyhedron* **2015**, *102*, 16–26. https://doi.org/10.1016/j.poly.2015.07.046.

(42) Yersin, H.; Gallhuber, E. On the Lowest Excited States of [Ru(Bpy)3](PF6)2 Single Crystals. *J. Am. Chem. Soc.* **1984**, *106* (22), 6582–6586. https://doi.org/10.1021/ja00334a022.

(43) Felix, F.; Ferguson, J.; Guedel, H. U.; Ludi, A. The Electronic Spectrum of Tris(2,2′-Bipyridine)Ruthenium(2+). *J. Am. Chem. Soc.* **1980**, *102* (12), 4096–4102. https://doi.org/10.1021/ja00532a019.

(44) Atkins, A. J.; Talotta, F.; Freitag, L.; Boggio-Pasqua, M.; González, L. Assessing Excited State Energy Gaps with Time-Dependent Density Functional Theory on Ru(II) Complexes. *J. Chem. Theory Comput.* **2017**, *13* (9), 4123–4145. https://doi.org/10.1021/acs.jctc.7b00379.

(45) Zhang, Y.; Thor, W.; Wong, K.-L.; Tanner, P. A. Determination of Triplet State Energy and the Absorption Spectrum for a Lanthanide Complex. *J. Phys. Chem. C* **2021**, *125* (13), 7022–7033. https://doi.org/10.1021/acs.jpcc.1c00158.

(46) Ward, M. D. Mechanisms of Sensitization of Lanthanide(III)-Based Luminescence in Transition Metal/Lanthanide and Anthracene/Lanthanide Dyads. *Coord. Chem. Rev.* **2010**, *254* (21), 2634–2642. https://doi.org/10.1016/j.ccr.2009.12.001.

(47) Charbonnière, L. J.; Faulkner, S.; Platas-Iglesias, C.; Regueiro-Figueroa, M.; Nonat, A.; Rodríguez-Blas, T.; de Blas, A.; Perry, W. S.; Tropiano, M. Ln2M Complexes (M = Ru, Re) Derived from a Bismacrocyclic Ligand Containing a 4,4′-Dimethyl-2,2′-Bipyridyl Bridging Unit. *Dalton Trans.* **2013**, *42* (10), 3667–3681. https://doi.org/10.1039/C2DT32660D.

(48) Faulkner, S.; Natrajan, L. S.; Perry, W. S.; Sykes, D. Sensitised Luminescence in Lanthanide Containing Arrays and d–f Hybrids. *Dalton Trans.* **2009**, No. 20, 3890–3899. https://doi.org/10.1039/B902006C.

(49) Berberan Santos, M. N.; Valeur, B. *Molecular Fluorescence: Principles and Applications, Second Edition*; 2012. https://doi.org/10.1002/9783527650002.

(50) Ishida, H.; Tobita, S.; Hasegawa, Y.; Katoh, R.; Nozaki, K. Recent Advances in Instrumentation for Absolute Emission Quantum Yield Measurements. *Coord. Chem. Rev.* **2010**, *254* (21), 2449–2458. https://doi.org/10.1016/j.ccr.2010.04.006.

(51) Baek, N. S.; Nah, M. K.; Kim, Y. H.; Kim, H. K. Ln(III)-Cored Complexes Based on 2-Thenoyltrifluoroacetone Ligand for near Infrared Emission: Energy Transfer Pathway and Transient Absorption Behavior. *J. Lumin.* **2007**, *127* (2), 707–712. https://doi.org/10.1016/j.jlumin.2007.03.020.

(52) Werts, M. H. V.; Jukes, R. T. F.; Verhoeven, J. W. The Emission Spectrum and the Radiative Lifetime of Eu3+ in Luminescent Lanthanide Complexes. *Phys Chem Chem Phys* **2002**, *4* (9), 1542–1548. https://doi.org/10.1039/B107770H.

(53) Pollnau, M.; Gamelin, D. R.; Lüthi, S. R.; Güdel, H. U.; Hehlen, M. P. Power Dependence of Upconversion Luminescence in Lanthanide and Transition-Metal-Ion Systems. *Phys Rev B* **2000**, *61* (5), 3337–3346. https://doi.org/10.1103/PhysRevB.61.3337.

(54) Zhang, L.; Yang, J.; Zhang, Z.; Yu, H.; Pan, W. Blue Cooperative Up-Conversion Luminescence of Yb:Y2O3 Transparent Ceramics. *Ceram. Int.* **2019**, *45* (7, Part A), 9278–9282. https://doi.org/10.1016/j.ceramint.2019.02.006.

Insert Table of Contents artwork here